ACS APPLIED MATERIALS & INTERFACES

Research Article

www.acsami.org

Facile Preparation of High-Quantum-Yield Gold Nanoclusters: Application to Probing Mercuric Ions and Biothiols

Heng-Chia Chang,[†] Ying-Feng Chang,[‡] Nien-Chu Fan,[‡] and Ja-an Annie Ho*[,†,‡]

[†]Department of Chemistry, National Tsing Hua University, No. 101, Sec. 2, Kuang-Fu Road, Hsinchu 30013, Taiwan

[‡]BioAnalytical Chemistry and Nanobiomedicine Laboratory, Department of Biochemical Science and Technology, National Taiwan University, No. 1, Sec. 4, Roosevelt Road, Taipei 10617, Taiwan

Supporting Information

ABSTRACT: This paper describes an eco-friendly, one-pot strategy for the synthesis of water-soluble, high-quantum-yield gold nanoclusters (AuNCs) stabilized with 11-mercaptoundecanoic acid (MUA) on their surfaces. The as-prepared ultrasmall MUA–AuNCs (1.9 nm) exhibited a quantum yield (QY) of 13%, higher than those of most previously described thiol-protected AuNCs. We applied these MUA–AuNCs as a versatile probe to develop a fluorescence "turn-off" assay for sensing Hg^{2+} ions as well as a fluorescence "turn-on" assay for sensing biothiols. The former assay operated through aggregation-induced fluorescence quenching upon interaction of the MUA–AuNCs with Hg^{2+} ions in a buffer containing 2,6-pyridinedicarboxylic acid (PDCA); this probe provided high sensitivity and remarkable selectivity over other selected metal ions with a limit of detection (LOD) for Hg^{2+} ions of 450 pM and linearity from 2 to 50 nM. In the latter assay for biothiols [i.e., cysteine (Cys), homocysteine (Hcy), glutathione (GSH)], the fluorescence of the Hg^{2+}–MUA–AuNCs complexes was turned on because the affinity of Hg^{2+} ions toward the SH group of the biothiols was greater than that toward the COOH groups of the MUA units on the surface of the AuNCs. This assay provided good linearity for the tested biothiols, ranging from 10 to 100 nM for Cys, from 10 to 100 nM for Hcy, and from 5 to 75 nM for GSH, with LODs of 5.4, 4.2, and 2.1 nM, respectively. In addition, these environmentally and biologically friendly AuNC probes tested satisfactorily against interference from a range of amino acids.

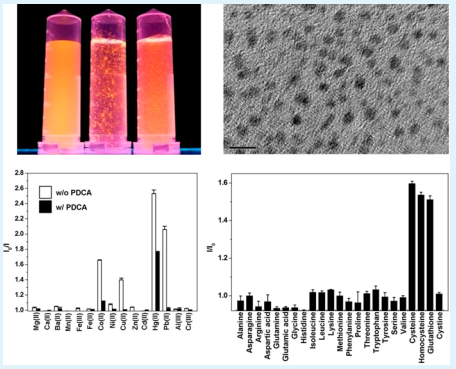

KEYWORDS: *high-quantum-yield gold nanoclusters, mercuric ion, biothiol, turn-on fluorescence sensor, turn-off fluorescence sensor*

1. INTRODUCTION

Luminescent metal (e.g., Au, Ag) nanoclusters having sizes comparable to the Fermi wavelength of the electron can exhibit moleculelike properties of discrete electronic states. Ultrafine Au nanoclusters (AuNCs) comprising several Au atoms display size-dependent photoluminescence and bright fluorescence.[1,2] As a result of their high photostability and biocompatibility, luminescent AuNCs have recently been recognized as promising candidates for in vitro/in vivo bioimaging,[3−6] sensing of metal ions,[7−9] and use in the fabrication of biosensors.[6,10,11] Over the past decade, several methods[12,13] involving strong stabilizing agents (e.g., poly(amidoamine), PAMAM) and reductants (e.g., $NaBH_4$) have been developed for the synthesis of luminescent AuNCs. For instance, PAMAM dendrimers incorporating AuNCs of various sizes (from Au_5 to Au_{31}) have exhibited various emission wavelengths ranging from the ultraviolet (UV) to the near-infrared (NIR).[12,13]

Glutathione (GSH) has been used as a capping agent to prepare luminescent AuNCs in the presence of $NaBH_4$.[14,15] The most thermodynamically stable GSH-protected AuNCs, $Au_{25}SG_{18}$, have been identified after separation through polyacrylamide gel electrophoresis (PAGE).[14,15] Furthermore, a frequently adopted route, ligand-induced etching, has enabled large Au nanoparticle precursors to be etched into small AuNCs through the action of polyethylenimine (PEI),[16] bovine serum albumin (BSA),[17] and thiols.[4,6,9,18] Nevertheless, because multistep procedures are mandatory for fabricating such Au-based nanomaterials, these processes can be complicated and time-consuming. Herein, we report a straightforward one-pot strategy, without the need for larger AuNP precursors or hazardous organic solvents (e.g., toluene,[4,18] MeOH[15]), for the preparation of high-quantum-yield AuNCs protected with 11-mercaptoundecanoic acid (MUA) on their surfaces; it involves the reduction of a mixture of MUA and Au^{3+} ions in the presence of $NaBH_4$. The resulting MUA–AuNCs exhibited a bright emission at 607 nm when irradiated with incident light at 330 nm [quantum yield (QY) = ca. 13%]. In addition, we could control the emission wavelength from the visible to the NIR by tuning the mole ratio of MUA to Au^{3+} ions.

The mercuric (Hg^{2+}) ion is a highly toxic pollutant that exists in water, soil, and the food chain; it can cause serious damage to the natural environment and poisoning in organisms.[19]

Received: July 16, 2014
Accepted: October 17, 2014
Published: October 17, 2014

   dx.doi.org/10.1021/am504546f | *ACS Appl. Mater. Interfaces* 2014, 6, 18824−18831

Therefore, demand exists to develop a detection method for the rapid and sensitive sensing of Hg^{2+} ions in our water supplies. Various sensing platforms for the detection of Hg^{2+} ions have been reported, including sensitive electrochemical method,[20] a strip biosensor based on toehold binding and exonuclease III-assisted signal amplification,[21] colorimetric assays employing AuNPs functionalized with various biolabels[22,23] as well as fluorescence methods exploiting organic dyes,[24,25] DNAs,[26,27] or semiconductor-based quantum dots (QDs).[28,29] Most of these methods, however, require complicated synthetic processes and exhibit low sensitivity. The luminescent MUA–AuNCs that we describe herein function as an indicator for the fluorescence "turn-off" detection of Hg^{2+} ions in the presence of 2,6-pyridinedicarboxylic acid (PDCA) with superb selectivity, operating based on particle aggregation–induced fluorescence quenching.

In addition, we have also verified the feasibility of using our as-prepared AuNCs as a sensing probe for physiologically important low-molecular-weight biothiols, namely cysteine (Cys), homocysteine (Hcy), and GSH, which play crucial roles in physiological systems (e.g., such cellular functions including detoxification, metabolism, and reversible redox reactions).[30] Cys is a risk factor for vascular diseases, including coronary heart disease and cerebrovascular disease.[31] High concentrations of Hcy in the blood can be associated with increased relative risks of coronary artery diseases, stroke, carotid vascular diseases, and Alzheimer's disease.[32,33] The lack of GSH in cells can increase cellular oxidative stress, which can lead to DNA damage and lipid oxidation.[34] As a result, the development of methods for rapid screening of the levels of these biothiols in biosamples would greatly assist both clinical diagnostics and research. The affinity of Hg^{2+} ions toward thiols is higher than that toward carboxylic acids.[35] Wang's group reported a detection assay for biothiols based on recovery of the fluorescence intensity of a QD–Hg^{2+} system.[36] In this study, we developed a sensitive and selective assay for the sensing of biothiols, based on the fluorescence "turn-on" of quenched Hg^{2+}–MUA–AuNC complexes. This assay has provided limits of detection (LODs) on the nanomolar level for the fluorescence detection of various biothiols.

2. EXPERIMENTAL SECTION

2.1. Reagents and Materials. All chemicals were of reagent grade or better. Cadmium nitrate, cobalt chloride hexahydrate, and nickel chloride were ordered from Wako (Osaka, Japan). Calcium chloride dehydrate, chromium nitrate nonahydrate, manganese sulfate, MUA, PDCA, acetonitrile, sodium borohydride, and sodium hydroxide were purchased from Sigma–Aldrich (St. Louis, MO). Copper chloride dihydrate, ferric chloride hexahydrate, ferrous chloride tetrahydrate, lead nitrate, mercuric nitrate monohydrate, sodium borate decahydrate, and zinc nitrate hexahydrate were obtained from J. T. Baker (Phillipsburg, NJ). Hydrogen tetrachloroaurate was acquired from Alfa Aesar (Ward Hill, MA). Hydrochloric acid and magnesium sulfate heptahydrate were purchased from Riedel–de Haën (Seelze, Germany). Nitric acid was obtained from Fluka (St. Louis, MO). Tris(2-carboxyethyl)phosphine (TCEP) was purchased from Invitrogen (Carlsbad, CA). All solutions were prepared using deionized water having a resistivity of no less than 18 MΩ cm^{-1} (Milli-Q, Bedford, MA).

2.2. Luminescent MUA–AuNCs. All pieces of glassware were cleaned in a bath of freshly prepared aqua regia [HCl:HNO_3, 3:1 (v/v)] and rinsed thoroughly in deionized water prior to use. Briefly, 10 mM MUA (2.0 mL, dissolved in 15 mM NaOH(aq)) was mixed with 5 mM $HAuCl_4$ (1.0 mL) to give a final MUA-to-Au^{3+} mole ratio of 4. An additional charge of NaOH (30 μmol) was added to the cloudy mixture of MUA and $HAuCl_4$. After the mixture became clear, the solution was subjected to vigorous stirring for 2 min and then a freshly prepared solution of $NaBH_4$ (2 mM, 250 μL) was added dropwise. The resulting solution was stirred continuously for 2 days at room temperature. MUA–AuNCs exhibiting different emission wavelengths were obtained by varying the MUA-to-$HAuCl_4$ mole ratio. Finally, excess reactants were removed by centrifugation (12 000 rpm, 20 min) through a centrifugal filter (molecular weight cutoff: 10 kDa). The as-prepared MUA–AuNCs were collected and stored at 4 °C prior to use.

2.3. Characterization of Luminescent MUA–AuNCs. The absorbance spectra of the MUA–AuNCs were recorded using a Cary 300 Bio UV–Vis spectrophotometer (Varian, Mulgrave, VIC, Australia). The excitation and emission spectra of the MUA–AuNCs were recorded using a Varian Cary Eclipse fluorescence spectrophotometer (Varian, Mulgrave, VIC, Australia). High-resolution transmission electron microscopy (HRTEM) images of the MUA–AuNCs were acquired using a JEOL JEM-2100 transmission electron microscope (Akishima, Tokyo, Japan). X-ray photoelectron spectroscopy (XPS) of the MUA–AuNCs (Au $4f_{7/2}$ orbitals) was conducted using an ULVAC-PHI XPS spectrometer (PHI Quantera SXM, Chigasaki, Japan).

2.4. Fluorescence "Turn-Off" Assay for Sensing Hg^{2+} Ions. An aliquot of MUA–AuNCs (1.5 mg/mL, 5 μL) were added to 5 mM sodium borate buffer (pH 10, 1 mL) containing various concentrations of Hg^{2+} ions and 5.0 μM PDCA. The solution was mixed thoroughly and then left at room temperature for 30 min. The fluorescence quenching spectra were then collected in the wavelength range 500–750 nm with excitation at 330 nm and maximum emission at 607 nm. The slit widths of the excitation and emission were both 5.0 nm. Interference of the fluorescence of the AuNCs was investigated in the presence of other metal ions individually.

Tap water was collected from our laboratory at National Tsing Hua University; it was subjected to centrifugation (16,000 rpm) and filtration through a 0.45-μm membrane to remove suspended particles prior to analysis. A series of water samples was prepared by spiking standard solutions (0.5 mL) of various concentrations of Hg^{2+} (5, 10, or 20 nM) in 10 mM sodium borate buffer (pH 10) and 10 μM PDCA into the treated tap water. The resulting solutions were then mixed with MUA–AuNC solutions (1.5 mg/mL, 5 μL). Incubation for 30 min was performed prior to recording the fluorescence spectra (excitation wavelength: 330 nm).

2.5. Fluorescence "Turn-On" Assay for Sensing Biothiols. An aliquot of MUA–AuNCs (1.5 mg/mL, 3 μL) were mixed thoroughly with Hg^{2+} solution (400 μM, 0.1 mL) for 30 min to quench fluorescence, followed by the addition of a biothiol (1 mL) solution of a desired concentration. The recovered fluorescence intensity was acquired using a fluorescence spectrophotometer operated with excitation at 330 nm and maximum emission at 607 nm. The selectivity toward the selected amino acids was determined using the same method as mentioned above.

Fresh human blood samples were obtained from personnel within our group. The conversion of disulfides to free thiols was performed based on a previously reported method:[37] TCEP (35 mM, 50 μL) was added to a plasma sample (500 μL), followed by incubation at 40 °C for 10 min and subsequent addition of acetonitrile (450 μL) as a precipitation agent. The treated blood samples were subjected to centrifugation (6000 rpm, 10 min). The supernatant containing the biothiols was collected and used for further analysis.

3. RESULTS AND DISCUSSION

3.1. Preparation of MUA–AuNCs. We developed a facile approach—using $NaBH_4$ to reduce Au^{3+} ions—for the preparation of luminescent MUA–AuNCs in a single step. To obtain good stability and dispersibility of the AuNCs in aqueous solution, we selected MUA as the capping agent, which we added to the reaction mixture. The carboxylic acid group of MUA enables further modification of the surfaces of the MUA–AuNCs with other functional molecules. To produce

ultrasmall AuNCs in the aqueous phase, we employed a relatively high thiol-to-Au ratio.[2] Because MUA has low solubility in water at pH 7 (ca. 1.1×10^{-5} g/mL), we dissolved it in alkaline NaOH (15 mM) to increase its solubility and accelerate MUA–AuNC synthesis in the aqueous phase (pH ~12). In this process, we first mixed MUA with Au^{3+} ions at a mole ratio of 4:1. The resulting mixture was cloudy as a result of neutralization between the alkaline solution of MUA and the acidic solution of $HAuCl_4$. Accordingly, we added a further charge of NaOH(aq) to enhance the solubility of the mixture of MUA and Au^{3+} ions in the aqueous phase. The color of mixed solution changed rapidly from yellow to colorless, indicating the formation of Au(I)–thiol complexes through the interaction of Au^{3+} ions with the thiol groups of MUA units.[38] Next, we used $NaBH_4$ to reduce the Au(I)–thiol complexes to form AuNCs. The HRTEM image in Figure 1A reveals that the resulting MUA–AuNCs were well dispersed, due to the presence of MUA units on the surfaces of the AuNCs efficiently inhibiting aggregation. The average diameter of the MUA–AuNCs was 1.9 ± 0.3 nm. Compared with the previously reported top-down approach (MUA employed to etch down larger AuNPs),[7] this bottom-up strategy for the preparation of AuNCs is simple and straightforward. Moreover, we did not observe the formation of larger AuNPs as byproducts, commonly observed in other synthetic strategies; accordingly, the size range of our AuNCs was much narrower than those obtained using previously reported methods.[12,16]

3.2. Optical Properties of MUA–AuNCs. Time-course measurements of the fluorescence evolution (see Figure S1 in the Supporting Information) revealed that the synthesis of MUA–AuNCs was complete within 2 days. Figure 1B presents the absorption spectrum of the MUA–AuNCs, illustrating the strong and broad absorption in the UV range with an onset at 350 nm. We attribute the peak at 240 nm to the MUA units on the surface of the AuNCs. The absence of a surface plasmon resonance peak near 520 nm in the spectrum indicates that the average core size of the formed AuNCs was less than 2.5 nm.[39] We observed strong fluorescence, centered at 607 nm, from the MUA–AuNCs (hereafter denoted MUA–AuNCs607) upon maximum excitation at 330 nm (Figure 1C). Orange light was emitted upon excitation with incident light at a wavelength of 302 nm from hand-held UV lamp (Figure 1C). The bright emission and theoretically low toxicity[40] (as compared to semiconductor-based quantum dots) of our Au-based fluorophores suggest their possible applicability in biological and environmental fields. Furthermore, the difference of 277 nm between the excitation and emission wavelengths decreases the potential interference from excitation, thereby increasing the intensity of the emission signal.

The mechanism behind the fluorescence of AuNCs has been proposed by several researchers testing various models. For instance, Whetten et al.[41] proposed that the fluorescence of AuNCs could be attributed to recombination among the ground state and two disparate excited states, so-called intraband and interband transitions. Murray et al.[42] suggested that the fluorescence of AuNCs is associated with interband transitions between the filled 5d band and the 6sp conduction band. Other studies have revealed that the fluorescence of the AuNCs is highly related to the presence of Au(I)–thiol complexes on the surface, with mechanisms ascribed to ligand-to-metal charge transfer (LMCT), ligand-to-metal-metal charge transfer (LMMCT), and ligand-to-metal NP core charge transfer (LMNCT).[7,39,41,43,44] By virtue of the similar spectral

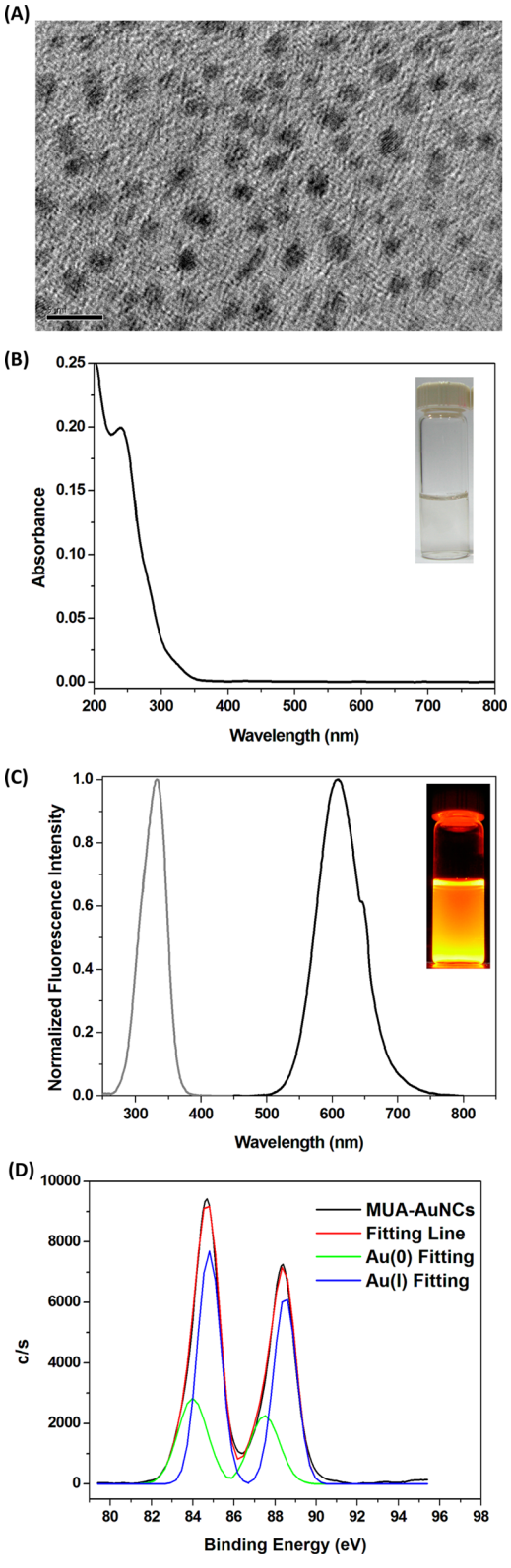

Figure 1. (A) HRTEM image of MUA–AuNCs (scale bar: 5 nm). (B) Absorbance spectrum of MUA–AuNCs. Inset: Photograph of MUA–AuNCs solution in room light. (C) Normalized fluorescence excitation (gray line) and emission (black line) spectra of MUA–AuNCs. Inset: Photograph of MUA–AuNCs solution under a hand-held UV lamp with excitation of 302 nm. (D) XPS spectra (Au 4f) of MUA–AuNCs607 (black line). XPS curve fitting revealed peaks at 84.0 and 84.8 eV, assigned to Au(0) (green line) and Au(I) (blue line), respectively.

behavior of Au(I)−alkanethiolates and our MUA−AuNCs607, we suspected the presence of Au(I) atoms in our sample.[43]

To confirm the existence of Au(I) atoms, we employed XPS to investigate the valence states of the Au atoms in MUA−AuNCs607. The XPS spectrum in Figure 1D reveals a maximum Au $4f_{7/2}$ binding energy (BE) for MUA−AuNCs607 of 84.7 eV (we used the BE of the alkyl chain C 1s orbital, 285.3 eV, as an internal reference), located between those of 84.0 eV for Au(0) and 85.1 eV for Au(I).[45] This finding suggests that Au(0) and Au(I) species coexisted in MUA−AuNCs607. After XPS curve fitting, we found two peaks at 84.0 and 84.8 eV, which we assign to Au(0) and Au(I) species, respectively. The ratio of the integrated areas of the fitting peaks suggested that the percentage of Au(I) in MUA−AuNCs607 was approximately 75%; therefore, we suspected that MUA−AuNCs607 comprised an ultrasmall Au(0) core enveloped by Au(I)−MUA shells, similar to the structures previously described for fluorescent GSH−AuNPs[46] and Au@Au(I)−thiomalate core@shell NPs.[47] When we further reacted MUA−AuNCs607 with excess $NaBH_4$, we assume that more of the Au(I) species were reduced to Au(0) atoms, with the fluorescence intensity decreasing by approximately 43%. Taken together, our findings indicated that the presence of Au(I)−MUA complexes in our AuNCs had an important effect on the fluorescence properties. The QY of MUA−AuNCs607 in aqueous solution, determined using rhodamine 6G (QY in EtOH: 0.95) as a standard,[4] was 13% (details shown in the Supporting Information); this value is comparable with the QYs of a number of semiconductor QDs,[48−50] but higher than those of most previously reported thiol-capped AuNCs.[4,7,8,10,41,51] Moreover, our method for synthesizing MUA−AuNCs607 provides a QY remarkably higher than those reported previously for fluorescent AuNCs stabilized with MUA.[7,52−55] Our present study also confirms that the QY can be enhanced significantly upon increasing the oxidation state of the Au atoms in the AuNCs[44] [MUA−AuNCs607 featured 75% of Au(I) atoms].

The fluorescence wavelength of our MUA−AuNCs could be tuned from the visible to the NIR by varying the mole ratio of the thiol to the Au^{3+} ions in the synthetic medium. For example, we obtained MUA−AuNCs754 (Em_{max} = 754 nm) and MUA−AuNCs814 (Em_{max} = 814 nm) species after adjusting the MUA/Au^{3+} mole ratio to 2.5 and 1.5, respectively. Figure S2 in the Supporting Information displays the absorbance and fluorescence spectra of MUA−AuNCs754 and MUA−AuNCs814. The particles in both MUA−AuNCs754 and MUA−AuNCs814 had average diameters similar to those in MUA−AuNCs607 (ca. 1.9 nm), suggesting that the red shifts in fluorescence were not dependent solely on the particle size (see Figure S4 in the Supporting Infomration). The low QYs of MUA−AuNCs754 and MUA−AuNCs814 (0.6 and 0.2%, respectively) presumably arose because the number of Au(I)−MUA species in these AuNCs was lower than that in MUA−AuNCs607. Notably, the QYs of AuNCs correlate highly to the number of Au(I)−thiol complexes.[56,57] The XPS spectra in Figure S5 in the Supporting Information reveal maximum Au $4f_{7/2}$ BEs at 84.6 eV for MUA−AuNCs754 and 84.5 eV for MUA−AuNCs814, values that are lower than that for MUA−AuNCs607 (84.7 eV). After curve fitting of the XPS spectra for Au(0) and Au(I) peaks, we calculated that approximately 55 and 45% of the Au atoms present in MUA−AuNCs754 and MUA−AuNCs814, respectively, were Au(I) species. The XPS data indicate that the QYs decreased upon decreasing the content of Au(I)−MUA complexes in the MUA−AuNCs. The different emission wavelengths in these MUA−AuNCs imply that the ground and excited states involved in the fluorescence process were affected significantly by the valence states of the Au atoms in the AuNCs.[44]

3.3. Fluorescence "Turn-Off" Assay for Sensing Hg^{2+} Ions. Because acidic functional groups (e.g., carboxylic acids) chelate metal ions with high stability constants (log K = 10.1 for Hg^{2+}),[23,58] we suspected that our MUA−AuNCs, without further modification, would sense Hg^{2+} ions in solution. Figure 2A reveals that the fluorescence intensity of MUA−AuNCs607 under a hand-held UV lamp with excitation of 302 nm was significantly quenched upon the addition of Hg^{2+} ions. Moreover, we observed agglomeration (Figure 2Ab), possibly because of complexation between Hg^{2+} ions and COOH groups of MUA units on the surface of MUA−AuNCs607. The maximum quenching of the MUA−AuNCs607 occurred after 30 min (Figure 2B). Accordingly, we suspected that MUA−AuNCs607 could be used as a luminescent probe for the

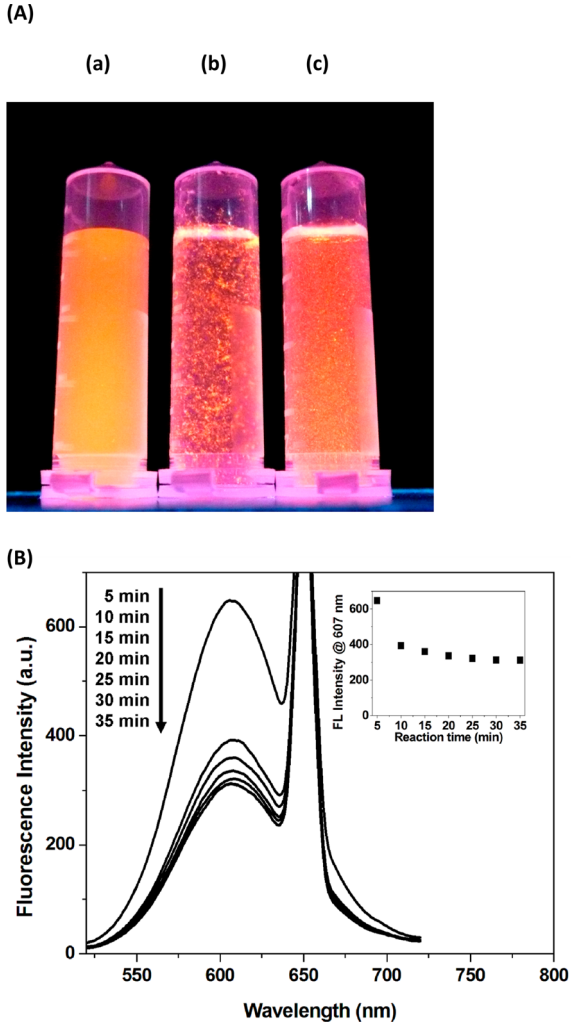

Figure 2. (A) Photograph of MUA−AuNCs607 (40 μg/mL) (a) in the absence of 170 μM Hg^{2+}; (b) in the presence of 170 μM Hg^{2+}; (c) after 10 mM Cys had been added to the sample in b (under a hand-held UV lamp with excitation of 302 nm). (B) Optimization of the incubation time for fluorescence quenching of AuNCs in the presence of Hg^{2+} ions.

detection of Hg^{2+} ions with a mechanism involving particle aggregation-induced fluorescence quenching.[7,8,59]

To investigate possible interference from other metal ions on the fluorescence quenching of MUA–AuNCs607, we tested the effects of Mg^{2+}, Ca^{2+}, Ba^{2+}, Mn^{2+}, Fe^{3+}, Fe^{2+}, Co^{2+}, Ni^{2+}, Cu^{2+}, Zn^{2+}, Cd^{2+}, Pb^{2+}, Al^{3+}, and Cr^{3+} ions under the same reaction conditions as described for the detection of Hg^{2+} ions. The white bars in Figure 3A reveal the interfering effects of these

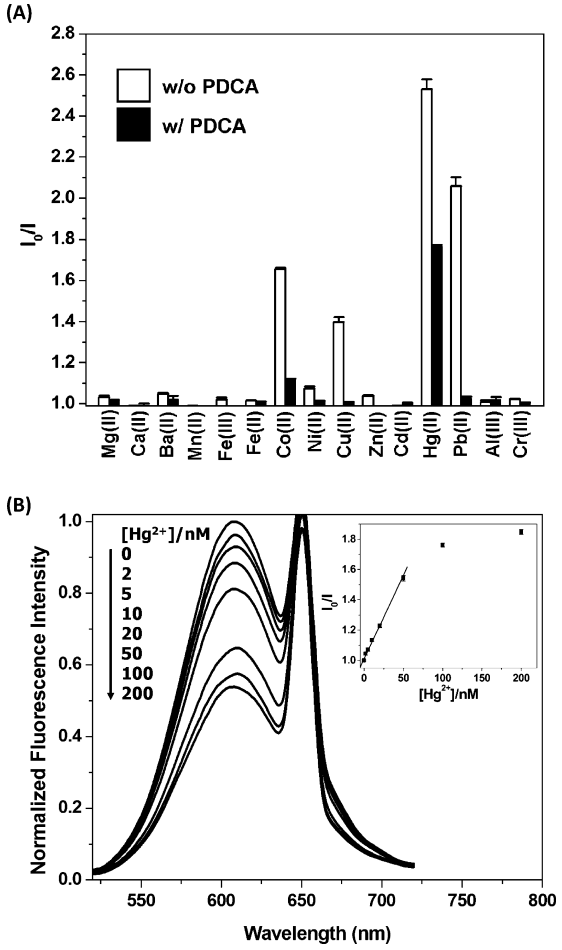

Figure 3. (A) Selectivity of the MUA–AuNCs toward 100 nM Hg^{2+}; measured in5 mM sodium borate buffer (pH 10) in the absence and presence of 5.0 μM PDCA (the concentration of each other selected metal ion was 500 nM). (B) Fluorescence spectrum of the MUA–AuNCs, revealing the quenching effect of Hg^{2+} ions at various concentrations ranging from 0 to 200 nM with an incubation time of 30 min. Inset: Dose–response plot, revealing the positive relationship between $[Hg^{+}]$ and the quenching of MUA–AuNCs at 607 nm (excitation wavelength, 330 nm; buffer, 5 mM sodium borate containing 5 μM PDCA).

metal ions (500 nM) on the fluorescence quenching of MUA–AuNCs607; from measurements of the values of $(I_0 - I)$, however, we observed poor selectivity for the Hg^{2+} fluorescence sensing probe. Therefore, we employed PDCA as a chelating agent to eliminate interference from other divalent metals to improve the selectivity of our sensor toward Hg^{2+} ions. The black bars in Figure 3A indicate the values of $(I_0 - I)$ determined in the presence of PDCA; we observe that the interference from other metals was restrained effectively, thereby ensuring selectivity in the detection of Hg^{2+} ions when using MUA–AuNCs607.

The fluorescence of MUA–AuNCs607 was quenched correspondingly upon increasing the concentration of Hg^{2+} ions (Figure 3B). We observed a good linear relationship between the value of I_0/I and the concentration of Hg^{2+} ions over the range from 2 to 50 nM (Figure 3B, inset); the fitted trend line can be expressed as $I_0/I = 1 + 1.1 \times 10^{-2}\,[Hg^{2+}]$ (R^2 = 0.990). The LOD for Hg^{2+} ions, based on a signal-to-noise ratio of 3, was 450 pM (0.1 ppb), suggesting that this probe is more sensitive than most previously developed AuNP– and fluorescent AuNC–based Hg^{2+} sensors;[7,23,60,61] moreover, this LOD is one twentieth of the maximum level of mercury in drinking water (10 nM, equivalent to 2 ppb) permitted by the United States Environmental Protection Agency (EPA). Thus, our AuNC probe has great potential for application in the detection of Hg^{2+} ions.

To test its practicality, we applied the proposed method to the analysis of the tap water samples spiked with Hg^{2+} ions. We employed a standard addition method to eliminate any matrix effects from the synthetic samples prepared with tap water. The fluorescence intensity of the MUA–AuNC probe decreased upon increasing the concentration of the standard solutions of Hg^{2+} ions spiked in the samples of tap water from 5 to 10 to 20 nM. The recoveries of the spiked tap water samples ranged from 97.9 ± 1.5% to 109.4 ± 4.5% (Table 1A). Relative

Table 1. (A) Recoveries from Tap Water Samples Spiked with Hg^{2+} Ions at pH 10 in 5 mM Sodium Borate Buffer Containing 5 μM PDCA; (B) Determination of Biothiols in Human Plasma

(A)			
tap water	spiked amount (nM)	found amount (nM)	recovery (%)
1	5	5.5 ± 0.2	109.4 ± 4.5
2	10	10.2 ± 0.3	101.5 ± 2.5
3	20	19.6 ± 0.3	97.9 ± 1.5

(B)				
plasma samples	biothiol originally presented in samples (μM)	spiked Cys (μM)	found Cys (μM)	recovery (%)
1	372.6	320	674.8 ± 4.0	97.4 ± 0.6
2		640	1143.4 ± 24	112.9 ± 2.3

standard deviations (RSDs) ranging from 1.1 to 4.1% verified the accuracy of this method and confirmed that the luminescent MUA–AuNC probe meets the testing requirements for environmental analyses.

3.4. Fluorescence "Turn-On" Assay for Sensing Biothiols. By virtue of the stability constants for Hg^{2+}–thiol complexes being higher than those of Hg^{2+}–carboxylic acid complexes,[35] we suspected that the aggregated Hg^{2+}–MUA–AuNC607 complexes would dissociate in the presence of thiols. Figure 2A(c) indicates that the large agglomerates of Hg^{2+}–MUA–AuNC607 complexes disassembled in the presence of Cys, with an associated by recovery in fluorescence. These phenomena enabled us to develop a fluorescence "turn-on" assay for the quantitative measurement of biothiols.

The fluorescence turn-on spectra in Figures 4A–C reveal that the fluorescence intensity of MUA–AuNC607 increased upon increasing the concentration of Cys, Hcy, and GSH, respectively. The insets present the fluorescence enhancements (I/I_0) plotted with respect to the concentrations of the biothiols; we observe good linear relationships in the ranges from 10 to 100 nM for Cys (R^2 = 0.985; RSDs: 0.4–2.2%),

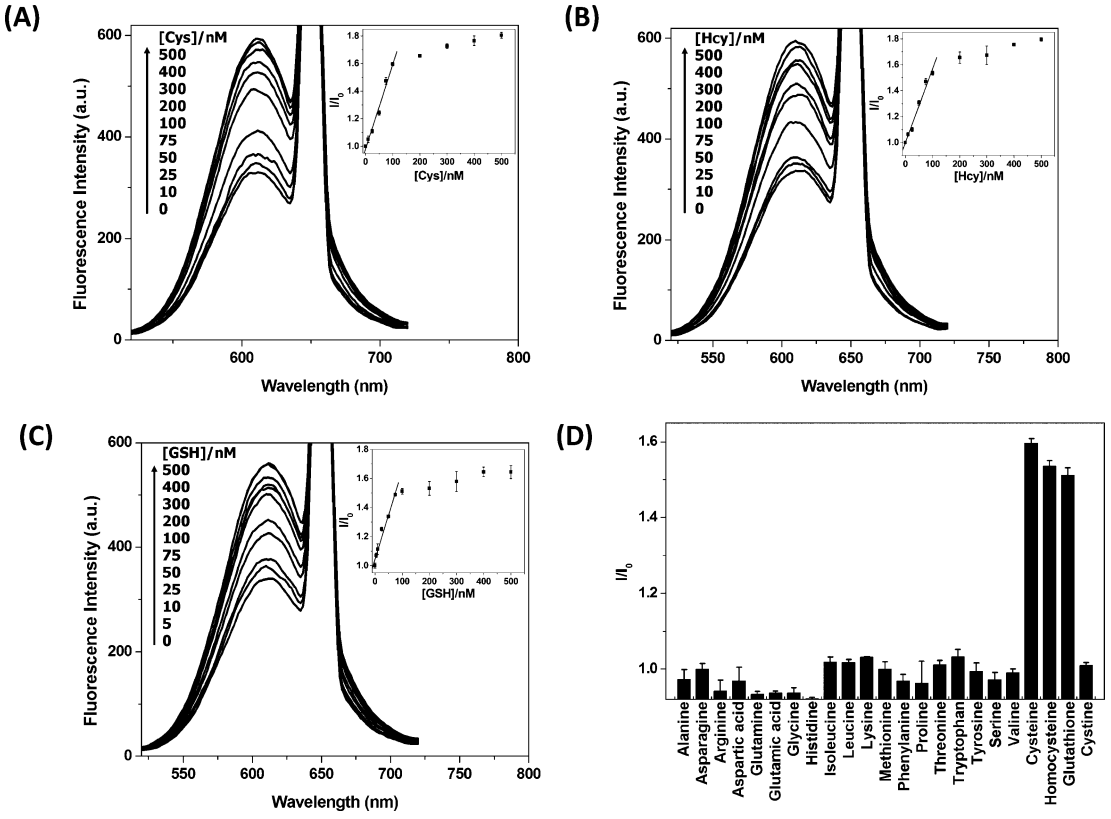

Figure 4. Fluorescence emission response profiles of Hg^{2+}−MUA−AuNC607 complexes in the presence of biothiols (concentrations: from 0 to 500 nM): (A) Cys, (B) Hcy, and (C) GSH. Insets: Relative fluorescence intensity (I/I_0, where I and I_0 are the fluorescence intensities of MUA−AuNC607 in the presence and absence, respectively. of biothiols at 607 nm) plotted with respect to the concentration of added biothiols. (D) Relative fluorescence intensity of Hg^{2+}−MUA−AuNC607 complexes in the presence of Cys, Hcy, and GSH (100 nM) and other selected amino acids (500 nM).

from 10 to 100 nM for Hcy (R^2 = 0.979; RSD: 0.8−1.7%), and from 5 to 75 nm for GSH (R^2 = 0.968; RSDs: 0.3−3.4%). The LODs of Cys, Hcy, and GSH were 5.4, 4.2, and 2.1 nM, respectively—all of which are much lower than their physiological concentrations in human fluids (ca. 250 μM of Cys in plasma; ca. 10 μM of Hcy in plasma; 1−10 mM of GSH in cells).[31,32,34] Furthermore, the sensitivity of this assay is comparable to, or even better than, those of previously proposed approaches for the sensing of biothiols.[36,62−64]

Next, we performed a study of the selectivity of our MUA−AuNC607-based sensor toward biothiols, examining the effects of selected amino acids at concentrations 5-fold higher than those of the tested biothiols. As indicated in Figure 4D, the presence of Cys, Hcy, or GSH resulted in a significant enhancement in fluorescence. In contrast, no obvious signal enhancements occurred in the presence of the selected amino acids at their higher concentrations. Furthermore, we also tested the effect of cystine, a molecule comprising two cysteine units linked through a disulfide bond. We observed a negligible increase of fluorescence in the presence of cystine, indicating that our proposed sensor provides a highly specific strategy for the sensing of biothiols.

The high efficiency, high sensitivity, and high selectivity of the Hg^{2+}−MUA−AuNC607 system toward biothiols suggested that our strategy might be directly extended to the detection of selected biothiols in biological samples. Accordingly, we examined of the presence of biothiols in human plasma, analyzing their concentrations through the standard addition method, with cysteine as the standard because of its high abundance in human plasma. The results in Table 1B reveal that our method has great potential for quantitative analysis of biothiols in real biological samples. Comparison of the present sensing probe with other AuNPs- and AuNC-based assays were summarized and provided in Supporting Information (Table 1S).

4. CONCLUSIONS

We have demonstrated a facile, one-pot, eco-friendly approach for the synthesis of water-soluble, high-QY MUA−AuNCs. These environmentally and biologically friendly AuNC probes feature several unique characteristics and attractive properties: (i) the synthetic process is clean and much simpler than previously reported etching-based strategies; (ii) the QYs of the MUA−AuNCs (up to 13%) are higher than those of previously reported thiol-capped AuNCs; (iii) rapid, ultrasensitive, label-free, selective fluorescence assays for the sensing of Hg^{2+} ions and biothiols can be developed from versatile MUA−AuNCs. Moreover, our luminescent MUA−AuNCs appear to be promising candidates for applications in bioimaging (biolabeling, biotracking), biosensing, and catalysis.

■ ASSOCIATED CONTENT

Supporting Information

Method for the determination of quantum yield of our luminescent MUA−AuNCs (MUA−AuNCs754), table summarized comparison of the present sensing probe with other AuNP- and AuNC-based assays, time evolution of the photoemission spectrum of our luminescent MUA−AuNCs

(MUA−AuNCs754), absorbance spectra and photographs of various MUA−AuNCs, XPS spectra (Au 4f) of various MUA−AuNCs. This material is available free of charge via the Internet at http://pubs.acs.org.

AUTHOR INFORMATION

Corresponding Author

*E-mail: jaho@ntu.edu.tw.

Notes

The authors declare no competing financial interest.

ACKNOWLEDGMENTS

This work was funded by the Ministry of Education of Taiwan (Aim for Top University Program) and grants from the Ministry of Science and Technology of Taiwan under contracts, 99-2923-M-002-008-MY2, 101-2113-M-002-003-MY3, and 102-2628-M-002-004-MY4. Authors wish to thank Ms. Amily Fang-ju Jou for valuable discussions.

REFERENCES

(1) Zheng, J.; Nicovich, P. R.; Dickson, R. M. Highly Fluorescent Noble-metal Quantum Dots. *Annu. Rev. Phys. Chem.* **2007**, *58*, 409−431.

(2) Jin, R. Quantum Sized, Thiolate-protected Gold Nanoclusters. *Nanoscale* **2010**, *2*, 343−362.

(3) Lin, S.-Y.; Chen, N.-T.; Sum, S.-P.; Lo, L.-W.; Yang, C.-S. Ligand Exchanged Photoluminescent Gold Quantum Dots Functionalized with Leading Peptides for Nuclear Targeting and Intracellular Imaging. *Chem. Commun.* **2008**, 4762−4764.

(4) Lin, C.-A. J.; Yang, T.-Y.; Lee, C.-H.; Huang, S. H.; Sperling, R. A.; Zanella, M.; Li, J. K.; Shen, J.-L.; Wang, H.-H.; Yeh, H.-I.; Parak, W. J.; Chang, W. H. Synthesis, Characterization, and Bioconjugation of Fluorescent Gold Nanoclusters Toward Biological Labeling Applications. *ACS Nano* **2009**, *3*, 395−401.

(5) Wu, X.; He, X.; Wang, K.; Xie, C.; Zhou, B.; Qing, Z. Ultrasmall Near-infrared Gold Nanoclusters for Tumor Fluorescence Imaging *in vivo*. *Nanoscale* **2010**, *2*, 2244−2249.

(6) Chen, C.-T.; Chen, W.-J.; Liu, C.-Z.; Chang, L.-Y.; Chen, Y.-C. Glutathione-bound Gold Nanoclusters for Selective-binding and Detection of Glutathione S-transferase-fusion Proteins from Cell Lysates. *Chem. Commun.* **2009**, 7515−7517.

(7) Huang, C.-C.; Yang, Z.; Lee, K.-H.; Chang, H.-T. Synthesis of Highly Fluorescent Gold Nanoparticles for Sensing Mercury(II). *Angew. Chem., Int. Ed.* **2007**, *46*, 6824−6828.

(8) Chen, W.; Tu, X.; Guo, X. Fluorescent Gold Nanoparticles-based Fluorescence Sensor for Cu^{2+} Ions. *Chem. Commun.* **2009**, 1736−1738.

(9) Xie, J.; Zheng, Y.; Ying, J. Y. Highly Selective and Ultrasensitive Detection of Hg^{2+} Based on Fluorescence Quenching of Au Nanoclusters by Hg^{2+}-Au^{+} interactions. *Chem. Commun.* **2010**, *46*, 961−963.

(10) Huang, C.-C.; Chen, C.-T.; Shiang, Y.-C.; Lin, Z.-H.; Chang, H.-T. Synthesis of Fluorescent Carbohydrate-Protected Au Nanodots for Detection of Concanavalin A and *Escherichia Coli*. *Anal. Chem.* **2009**, *81*, 875−882.

(11) Wen, F.; Dong, Y.; Feng, L.; Wang, S.; Zhang, S.; Zhang, X. Horseradish Peroxidase Functionalized Fluorescent Gold Nanoclusters for Hydrogen Peroxide Sensing. *Anal. Chem.* **2011**, *83*, 1193−1196.

(12) Zheng, J.; Zhang, C.; Dickson, R. M. Highly Fluorescent, Water-soluble, Size-tunable Gold Quantum Dots. *Phys. Rev. Lett.* **2004**, *93*, 077402.

(13) Zheng, J.; Petty, J. T.; Dickson, R. M. High Quantum Yield Blue Emission from Water-soluble Au-8 Nanodots. *J. Am. Chem. Soc.* **2003**, *125*, 7780−7781.

(14) Negishi, Y.; Takasugi, Y.; Sato, S.; Yao, H.; Kimura, K.; Tsukuda, T. Magic-numbered Au-n clusters Protected by Glutathione Monolayers (n=18, 21, 25, 28, 32, 39): Isolation and Spectroscopic Characterization. *J. Am. Chem. Soc.* **2004**, *126*, 6518−6519.

(15) Negishi, Y.; Nobusada, K.; Tsukuda, T. Glutathione-protected Gold Clusters Revisited: Bridging the Gap Between Gold(I)-thiolate Complexes and Thiolate-protected Gold Nanocrystals. *J. Am. Chem. Soc.* **2005**, *127*, 5261−5270.

(16) Duan, H.; Nie, S. Etching Colloidal Gold Nanocrystals with Hyperbranched and Multivalent Polymers: A New Route to Fluorescent and Water-soluble Atomic Clusters. *J. Am. Chem. Soc.* **2007**, *129*, 2412−2413.

(17) Habeeb Muhammed, M. A.; Verma, P. K.; Pal, S. K.; Retnakumari, A.; Koyakutty, M.; Nair, S.; Pradeep, T. Luminescent Quantum Clusters of Gold in Bulk by Albumin-Induced Core Etching of Nanoparticles: Metal Ion Sensing, Metal-Enhanced Luminescence, and Biolabeling. *Chem.—Eur. J.* **2010**, *16*, 10103−10112.

(18) Muhammed, M. A. H.; Verma, P. K.; Pal, S. K.; Kumar, R. C. A.; Paul, S.; Omkumar, R. V.; Pradeep, T. Bright, NIR-Emitting Au-23 from Au-25: Characterization and Applications Including Biolabeling. *Chem.—Eur. J.* **2009**, *15*, 10110−10120.

(19) Järup, L. Hazards of Heavy Metal Contamination. *Br. Med. Bull.* **2003**, *68*, 167−182.

(20) Xuan, F.; Luo, X.; Hsing, I. M. Conformation-Dependent Exonuclease III Activity Mediated by Metal Ions Reshuffling on Thymine-Rich DNA Duplexes for an Ultrasensitive Electrochemical Method for Hg^{2+} Detection. *Anal. Chem.* **2013**, *85*, 4586−4593.

(21) Chen, J.; Zhou, S.; Wen, J. Disposable Strip Biosensor for Visual Detection of Hg^{2+} Based on Hg^{2+}-triggered Toehold Binding and Exonuclease III-Assisted Signal Amplification. *Anal. Chem.* **2014**, *86*, 3108−3114.

(22) Zhao, W.; Brook, M. A.; Li, Y. Design of Gold Nanoparticle-based Colorimetric Biosensing Assays. *Chembiochem* **2008**, *9*, 2363−2371.

(23) Knecht, M.; Sethi, M. Bio-inspired Colorimetric Detection of Hg^{2+} and Pb^{2+} Heavy Metal Ions Using Au Nanoparticles. *Anal. Bioanal. Chem.* **2009**, *394*, 33−46.

(24) Dickerson, T. J.; Reed, N. N.; LaClair, J. J.; Janda, K. D. A Precipitator for the Detection of Thiophilic Metals in Aqua. *J. Am. Chem. Soc.* **2004**, *126*, 16582−16586.

(25) Rurack, K.; Kollmannsberger, M.; Resch-Genger, U.; Daub, J. A selective and Sensitive Fluoroionophore for Hg(II), Ag(I), and Cu(II) with Virtually Decoupled Fluorophore and Receptor Units. *J. Am. Chem. Soc.* **2000**, *122*, 968−969.

(26) Xiang, Y.; Wang, Z.; Xing, H.; Wong, N. Y.; Lu, Y. Label-free Fluorescent Functional DNA Sensors Using Unmodified DNA: A Vacant Site Approach. *Anal. Chem.* **2010**, *82*, 4122−4129.

(27) Wang, H.; Wang, Y.; Jin, J.; Yang, R. Gold Nanoparticle-based Colorimetric and "Turn-On" Fluorescent Probe for Mercury(II) Ions in Aqueous Solution. *Anal. Chem.* **2008**, *80*, 9021−9028.

(28) Wang, Y.; Li, J.; Jin, J.; Wang, H.; Tang, H.; Yang, R.; Wang, K. Strategy for Molecular Beacon Binding Readout: Separating Molecular Recognition Element and Signal Reporter. *Anal. Chem.* **2009**, *81*, 9703−9709.

(29) Page, L. E.; Zhang, X.; Jawaid, A. M.; Snee, P. T. Detection of Toxic Mercury Ions Using a Ratiometric CdSe/ZnS Nanocrystal Sensor. *Chem. Commun.* **2011**, *47*, 7773−7775.

(30) Townsend, D. M.; Tew, K. D.; Tapiero, H. Sulfur Containing Amino Acids and Human Disease. *Biomed. Pharmacother.* **2004**, *58*, 47−55.

(31) El-Khairy, L.; Ueland, P. M.; Refsum, H.; Graham, I. M.; Vollset, S. E. Plasma Total Cysteine as A Risk Factor for Vascular Disease - The European Concerted Action Project. *Circulation* **2001**, *103*, 2544−2549.

(32) Christen, W. G.; Ajani, U. A.; Glynn, R. J.; Hennekens, C. H. Blood Levels off Homocysteine and Increased Risks of Cardiovascular Disease - Causal of Casual? *Arch. Int. Med.* **2000**, *160*, 422−434.

(33) Seshadri, S.; Beiser, A.; Selhub, J.; Jacques, P. F.; Rosenberg, I. H.; D'Agostino, R. B.; Wilson, P. W. F.; Wolf, P. A. Plasma Homocysteine as A Risk Factor for Dementia and Alzheimer's Disease. *N. Engl. J. Med.* **2002**, *346*, 476−483.

(34) Schulz, J. B.; Lindenau, J.; Seyfried, J.; Dichgans, J. Glutathione, Oxidative Stress and Neurodegeneration. *Eur. J. Biochem.* **2000**, *267*, 4904−4911.
(35) Mahalingam, R. Interactions Between Mercury and Dissolved Organic Matter - A Review. *Chemosphere* **2004**, *55*, 319−331.
(36) Han, B.; Yuan, J.; Wang, E. Sensitive and Selective Sensor for Biothiols in the Cell based on the Recovered Fluorescence of the CdTe Quantum Dots-Hg(II) System. *Anal. Chem.* **2009**, *81*, 5569−5573.
(37) Zhang, N.; Qu, F.; Luo, H. Q.; Li, N. B. Sensitive and Selective Detection of Biothiols Based on Target-induced Agglomeration of Silver Nanoclusters. *Biosens. Bioelectron.* **2013**, *42*, 214−218.
(38) Corbierre, M. K.; Lennox, R. B. Preparation of Thiol-capped Gold Nanoparticles by Chemical Reduction of Soluble Au(I)-thiolates. *Chem. Mater.* **2005**, *17*, 5691−5696.
(39) Duff, D. G.; Baiker, A.; Edwards, P. P. A New Hydrosol of Gold Clusters 1. Formation and Particle-size Variation. *Langmuir* **1993**, *9*, 2301−2309.
(40) Zhang, X. D.; Wu, D.; Shen, X.; Liu, P. X.; Fan, F. Y.; Fan, S. J. *In vivo* Renal Clearance, Biodistribution, Toxicity of Gold Nanoclusters. *Biomaterials* **2012**, *33*, 4628−4638.
(41) Link, S.; Beeby, A.; FitzGerald, S.; El-Sayed, M. A.; Schaaff, T. G.; Whetten, R. L. Visible to Infrared Luminescence from a 28-atom Gold Cluster. *J. Phys. Chem. B* **2002**, *106*, 3410−3415.
(42) Huang, T.; Murray, R. W. Visible Luminescence of Water-soluble Monolayer-protected Gold Clusters. *J. Phys. Chem. B* **2001**, *105*, 12498−12502.
(43) Cha, S.-H.; Kim, J.-U.; Kim, K.-H.; Lee, J.-C. Preparation and Photoluminescent Properties of Gold(I)-alkanethiolate Complexes Having Highly Ordered Supramolecular Structures. *Chem. Mater.* **2007**, *19*, 6297−6303.
(44) Wu, Z.; Jin, R. On the Ligand's Role in the Fluorescence of Gold Nanoclusters. *Nano Lett.* **2010**, *10*, 2568−2573.
(45) Xie, J.; Zheng, Y.; Ying, J. Y. Protein-directed Synthesis of Highly Fluorescent Gold Nanoclusters. *J. Am. Chem. Soc.* **2009**, *131*, 888−889.
(46) Zhou, C.; Sun, C.; Yu, M.; Qin, Y.; Wang, J.; Kim, M.; Zheng, J. Luminescent Gold Nanoparticles with Mixed Valence States Generated from Dissociation of Polymeric Au(I) Thiolates. *J. Phys. Chem. C* **2010**, *114*, 7727−7732.
(47) Corthey, G. n.; Giovanetti, L. J.; Ramallo-López, J. M.; Zelaya, E.; Rubert, A. A.; Benitez, G. A.; Requejo, F. l. G.; Fonticelli, M. H.; Salvarezza, R. C. Synthesis and Characterization of Gold@Gold(I) - Thiomalate Core@Shell Nanoparticles. *ACS Nano* **2010**, *4*, 3413−3421.
(48) Sondi, I.; Siiman, O.; Matijević, E. Synthesis of CdSe Nanoparticles in the Presence of Aminodextran as Stabilizing and Capping Agent. *J. Colloid Interface Sci.* **2004**, *275*, 503−507.
(49) Williams, J. V.; Adams, C. N.; Kotov, N. A.; Savage, P. E. Hydrothermal Synthesis of CdSe Nanoparticles. *Ind. Eng. Chem. Res.* **2007**, *46*, 4358−4362.
(50) Roy, M. D.; Herzing, A. A.; De Paoli Lacerda, S. H.; Becker, M. L. Emission-tunable Microwave Synthesis of Highly Luminescent Water Soluble CdSe/ZnS Quantum Dots. *Chem. Commun.* **2008**, 2106−2108.
(51) Shang, L.; Dorlich, R. M.; Brandholt, S.; Schneider, R.; Trouillet, V.; Bruns, M.; Gerthsen, D.; Nienhaus, G. U. Facile Preparation of Water-soluble Fluorescent Gold Nanoclusters for Cellular Imaging Applications. *Nanoscale* **2011**, *3*, 2009−2014.
(52) Sun, J.; Zhang, J.; Jin, Y. 11-Mercaptoundecanoic Acid Directed One-pot Synthesis of Water-soluble Fluorescent Gold Nanoclusters and Their Use as Probes for Sensitive and Selective Detection of Cr^{3+} and Cr^{6+}. *J. Mater. Chem. C* **2013**, *1*, 138−143.
(53) Guo, Y.; Wang, Z.; Shao, H.; Jiang, X. Stable Fluorescent Gold Nanoparticles for Detection of Cu^{2+} with Good Sensitivity and Selectivity. *Analyst* **2012**, *137*, 301−304.
(54) Sun, J.; Yue, Y.; Wang, P.; He, H.; Jin, Y. Facile and Rapid Synthesis of Water-soluble Fluorescent Gold Nanoclusters for Sensitive and Selective Detection of Ag^{+}. *J. Mater. Chem. C* **2013**, *1*, 908−913.
(55) He, Y.; Wang, X.; Zhu, J.; Zhong, S.; Song, G. Ni^{2+}-modified Gold Nanoclusters for Fluorescence Turn-on Detection of Histidine in Biological Fluids. *Analyst* **2012**, *137*, 4005−4009.
(56) Wang, G.; Guo, R.; Kalyuzhny, G.; Choi, J.-P.; Murray, R. W. NIR Luminescence Intensities Increase Linearly with Proportion of Polar Thiolate Ligands in Protecting Monolayers of Au-38 and Au-140 Quantum Dots. *J. Phys. Chem. B* **2006**, *110*, 20282−20289.
(57) Shiang, Y.-C.; Huang, C.-C.; Chang, H.-T. Gold Nanodot-based Luminescent Sensor for the Detection of Hydrogen Peroxide and Glucose. *Chem. Commun.* **2009**, 3437−3439.
(58) Huang, C.-C.; Chang, H.-T. Parameters for Selective Colorimetric Sensing of Mercury(II) in Aqueous Solutions Using Mercaptopropionic Acid-modified Gold Nanoparticles. *Chem. Commun.* **2007**, 1215−1217.
(59) Adhikari, B.; Banerjee, A. Facile Synthesis of Water-Soluble Fluorescent Silver Nanoclusters and Hg-II Sensing. *Chem. Mater.* **2010**, *22*, 4364−4371.
(60) Wei, H.; Wang, Z.; Yang, L.; Tian, S.; Hou, C.; Lu, Y. Lysozyme-stabilized Gold Fluorescent Cluster: Synthesis and Application as Hg^{2+} Sensor. *Analyst* **2010**, *135*, 1406−1410.
(61) Hu, D.; Sheng, Z.; Gong, P.; Zhang, P.; Cai, L. Highly Selective Fluorescent Sensors for Hg^{2+} Based on Bovine Serum Albumin-capped Gold Nanoclusters. *Analyst* **2010**, *135*, 1411−1416.
(62) Shang, L.; Qin, C.; Wang, T.; Wang, M.; Wang, L.; Dong, S. Fluorescent Conjugated Polymer-stabilized Gold Nanoparticles for Sensitive and Selective Detection of Cysteine. *J. Phys. Chem. C* **2007**, *111*, 13414−13417.
(63) Zhang, Y.; Li, Y.; Yan, X.-P. Photoactivated CdTe/CdSe Quantum Dots as a Near Infrared Fluorescent Probe for Detecting Biothiols in Biological Fluids. *Anal. Chem.* **2009**, *81*, 5001−5007.
(64) Chen, S.-J.; Chang, H.-T. Nile Red-adsorbed Gold Nanoparticles for Selective Determination of Thiols based on Energy Transfer and Aggregation. *Anal. Chem.* **2004**, *76*, 3727−3734.